Effect of metal cation replacement on the electronic structure of metalorganic halide perovskites: Replacement of lead with alkaline-earth metals

Meysam Pazoki,[1,*] T. Jesper Jacobsson,[2] Anders Hagfeldt,[2] Gerrit Boschloo,[1] and Tomas Edvinsson[3,†]

[1]*Department of Chemistry, Ångström Laboratory, Uppsala University, Box 538, 75121 Uppsala, Sweden*

[2]*Laboratory of Photomolecular Science, Department of Chemistry and Chemical Engineering, Swiss Federal Institute of Technology, Station 6, CH-1015 Lausanne, Switzerland*

[3]*Department of Engineering Sciences–Solid State Physics, Uppsala University, Box 534, 75121 Uppsala, Sweden*

(Received 15 January 2016; revised manuscript received 11 February 2016; published 7 April 2016)

Organic and inorganic lead halogen perovskites, and in particular, $CH_3NH_3PbI_3$, have during the last years emerged as a class of highly efficient solar cell materials. Herein we introduce metalorganic halogen perovskite materials for energy-relevant applications based on alkaline-earth metals. Based on the classical notion of Goldschmidt's rules and quantum mechanical considerations, the three alkaline-earth metals, Ca, Sr, and Ba, are shown to be able to exchange lead in the perovskite structure. The three alkaline-earth perovskites, $CH_3NH_3CaI_3$, $CH_3NH_3SrI_3$, and $CH_3NH_3BaI_3$, as well as the reference compound, $CH_3NH_3PbI_3$, are in this paper investigated with density functional theory (DFT) calculations, which predict these compounds to exist as stable perovskite materials, and their electronic properties are explored. A detailed analysis of the projected molecular orbital density of states and electronic band structure from DFT calculations were used for interpretation of the band-gap variations in these materials and for estimation of the effective masses of the electrons and holes. Neglecting spin-orbit effects, the band gap of $MACaI_3$, $MASrI_3$, and $MABaI_3$ were estimated to be 2.95, 3.6, and 3.3 eV, respectively, showing the relative change expected for metal cation exchange. The shifts in the conduction band (CB) edges for the alkaline-earth perovskites were quantified using scalar relativistic DFT calculations and tight-binding analysis, and were compared to the situation in the more extensively studied lead halide perovskite, $CH_3NH_3PbI_3$, where the change in the work function of the metal is the single most important factor in tuning the CB edge and band gap. The results show that alkaline-earth-based organometallic perovskites will not work as an efficient light absorber in photovoltaic applications but instead could be applicable as charge-selective contact materials. The rather high CB edge and the wide band gap together with the large difference of the electron and hole effective masses make them good candidates for *n*-type selective layers in hot carrier injection solar cell devices together with some light absorber candidates. The fact that they have similar lattice constants as the lead perovskite and suitable positions of the valence band edges open up the possibility to use them also as thin epitaxial *p*-type hole selective contacts in combination with the lead halogen perovskite materials. This can lead to both charge selectivity as well as to superior crystal growth of lead perovskite with less contact stress, which is interesting for further investigations.

DOI: 10.1103/PhysRevB.93.144105

I. INTRODUCTION

Solar energy is an environmentally friendly and sustainable energy source capable to cover a significant part of our future energy demands. A class of solar cell materials that has gained a lot of attention in the last few years is the organometallic lead halide perovskites, with record device efficiencies now reaching higher than 20% [1–3]. Introduced in solid-state devices in 2012 [4,5], the perovskite solar cells have the highest rate of solar cell efficiency improvement ever seen, and in the last five years they have gone from a curiosity into a technology that in terms of power conversion efficiency are able to compete with more than 20-year-old technologies such as copper indium gallium selenide (CIGS) solar cells [6]. Although they have reached decent efficiencies with simple solution processed fabrication methods, which in principle fairly easily can be scaled up to roll-to-roll printing systems, further progress is needed to truly pave their way towards the competitive market place for solar cell devices. Device stability [7–10], fundamental underlying device physics [11–13], and environmental concerns about lead toxicity [9,14,15] are examples of open issues and pitfalls which require more research.

Halide perovskite materials have the general formula AMX_3, where A is a cation, M is a metal cation, and X is a halide such as I or Br. In solar cells, the perovskite is implemented in the device as a few hundred nanometer thick light-absorbing layer sandwiched between an electron and a hole selective contact [16]. Methyl ammonium lead iodine perovskite $CH_3NH_3PbI_3$, hereafter abbreviated $MAPbI_3$, could be seen as the model compound in the class of lead halogen perovskites. That is the compound that so far has attracted the largest interest, and even if the current record devices mix in some formamidinium ions and bromide in the structure, most of the reported high-efficiency devices are based on $CH_3NH_3PbI_3$. Replacing the methyl ammonium (MA) with different cations [17–20], the lead with different metal cations [14,15,21], and the iodine with other halogens [22,23] is in the center of current research interests in order to modify the material properties [24] in order to understand the material and

*meysam.pazoki@kemi.uu.se

†tomas.edvinsson@angstrom.uu.se

 ©2016 American Physical Society

device physics [25–28], improve the device efficiency [2,6], and to replace the toxic lead with a more environmentally friendly element [14,15].

According to Goldschmidt´s rules [29], cations with a similar size and with the same charge as Pb^{2+} would be interesting candidates for replacing the lead. The tolerance factor from experimentally determined ionic radii is an essential parameter for prediction of new perovskite compounds and their crystalline phase and has been reported for a large variety of organic-inorganic perovskites in Ref. [30]. The effect of the difference in electronegativity and quantum mechanical considerations, however, also have to be considered where, for example, Cu^{+} and Na^{+} do not substitute each other in compounds due to the different electronic structure and thus the large difference in electronegativity. In a previous paper [15] we pointed out that Sr^{2+} has a nearly identical ionic radius with Pb^{2+} and also an electronic structure allowing sixfold coordination [15], and therefore should be able to replace lead in the perovskite structure. DFT calculations revealed that the strontium perovskite, $MASrI_3$, is a stable phase but that the band gap is too large to be an efficient photoabsorber in the solar spectrum.

The key results from our previous study were that lead could be replaced by strontium and still form a stable perovskite structure, despite the large difference in electronegativity, but that the band gap of that structure is too high for absorption purposes in photovoltaic applications. The ionic character of the bonds and the lack of *d* orbitals in the $MASrI_3$ valence band (VB) make the VB dispersion very small, which indicates a large effective mass for the holes. The electron effective mass was, however, estimated to be reasonably low. The material could then work quite well as an electron selective material.

In particular, it would be interesting to see how the electronic and optical properties vary for the set of alkaline-earth halogen perovskites where the possibility of tuning the position of the conduction band (CB) and VB edges are of direct importance for application as charge-carrier selective materials.

Following our previous work [15], we here investigate the stability and electronic effects of replacing lead in $MAPbI_3$ with different alkaline-earth-metal cations. Density functional theory (DFT) calculations are used to predict stable perovskite crystals with AMX_3 formulas where X is Ca, Sr, or Ba.

Although structural properties of the Pb [27,31,32] and alkaline-earth-metal [33] perovskite materials have been investigated by GGA-DFT and show satisfactory agreement with experimental values, there are still possible inaccuracies for the DFT predicted band-gap values. Scalar relativistic DFT with a GGA functional are shown to predict the experimental band gap of $MAPbI_3$ correctly [32], without implementation of spin-orbit coupling (SOC) by which the gap is underestimated for $MAPbI_3$ [34,35]. De Angelis *et al.* have investigated band-gap variation of both $MASnI_3$ and $MAPbI_3$ using scalar relativistic GW calculations and compared that with SOC-DFT and scalar relativistic GGA [35]. Scalar relativistic effects predict the band gap of Pb perovskites well while they underestimate the band gap for Sn perovskites. This is due to relativistic effects within the heavy metal lead that play a role for reproducing the correct experimental band-gap value. In the view of the different effects expected for the different approaches, we have here used the GGA approximation for $MAPbI_3$ on a scalar relativistic level for comparison with the alkaline-earth perovskite materials, which previously have been shown to have better agreement with experiments compared to SOC calculations for lead and tin perovskite materials [35–37].

Reported band gaps may include the well-known band-gap problem of pure DFT, while a cancelation of effects can be expected when using a combination of SOC and methods with more exact exchange, such as hybrid DFT and GW. In either case, by following a consistent scheme, the trends for different metals can be distinguished [31] and can give insights to not only understanding of the general trends with metal exchange in organic perovskite materials, but also insights into the mechanism of change in the electronic structure, useful for future engineering of these not-yet-synthesized charge-selective materials.

Analysis of partial density of states, charge density, atomic Löwdin charges, and distribution of total potential within the lattice gives insights to band-edge shifts and band-gap variations of these materials in comparison to $MAPbI_3$ and helps further understanding of band-gap engineering of the metal-halogen perovskite materials. The calculated electronic structures predict the alkaline-earth perovskite to be viable candidates as both thin *p*-type hole selective contacts in halogen perovskite solar cells as well as electron selective contacts in hot carrier injection solar cells.

Initial experimental efforts to synthesize the methyl ammonium barium iodide ($MABaI_3$), methyl ammonium strontium iodide ($MASrI_3$), and methyl ammonium calcium iodide ($MACaI_3$) with solution-based techniques were unsuccessful due to an extreme sensitivity to humidity as well as solubility difficulties of the precursors, in contrast to the situation for $MAPbI_3$. However, as suggested previously, a vapor phase growth should instead be a more promising approach for the synthesis of these compounds [15].

II. THEORETICAL MODELS AND METHODS

Periodic DFT calculations were performed with the QUANTUM ESPRESSO package [38] on resources provided by the Swedish National Infrastructure for Computing (SNIC) through the Uppsala Multidisciplinary Center for Advanced Computational Science (UPPMAX).

The crystal DFT calculations were performed using the general gradient approximation (GGA) exchange correlation functional [39] and the Perdew-Burke-Ernzerhof (PBE) [40] pseudopotential. The barium $5s^2/5p^6/6s^2$, the calcium $3s^2/3p^6/4s^2$, the strontium $4s^2/4p^6/5s^2$, the lead $5d^{10}/6s^2/6p^2$, the nitrogen $2s^2/2p^3$, the iodide $5s^2/5p^5$, and the carbon $2s^2/2p^2$ electrons were considered as valence electrons. The super cells consisted of 48 atoms in a tetragonal Bravais lattice, and the starting cell parameters were set to $a = 8.71$ Å and $c = 12.46$ Å. The orientation of the different methyl ammonium ions ($CH_3NH_3^{+}$) was chosen in a way where neighboring dipoles were perpendicular to each other. This configuration of the methyl ammonium ions has been reported to constitute, according to DFT calculations, the most stable phase at room temperature for the lead perovskite $CH_3NH_3PbI_3$ [32]. This is in line with experimental data showing a tetragonal structure with semirandom orientation

of the methyl ammonium ions at room temperature for the lead iodine perovskite. This structure could be described as composed of four slightly distorted cubic unit cells with a cell parameter a around 6.31 Å.

All the unit-cell vectors and atom coordinates were relaxed to have a total force lower than 0.08 Ry/a.u. The XCRYSDEN package [41] was used for visualization of atoms, potentials, and charge densities. Cutoff energies for the plane wave function and the charge density were set to 35 and 350 Rydberg, respectively. Brillouin zone samplings were carried out by a $3 \times 3 \times 3$ Monkhorst-Pack grid (MPG) for the relaxation procedure, a $4 \times 4 \times 4$ MPG for the self-consistent procedures, and a $6 \times 6 \times 6$ MPG for the non-self-consistent procedures.

The difference in formation energy between the barium, calcium, strontium, and the lead perovskites was estimated by calculating the difference of their total lattice energy and subtracting the energy difference of the lead and alkaline-earth elements while considering the same thermodynamic growth factor for both lattices [15]. The single atom energies were calculated using the same computational parameters, except that single elements of Pb, Ba, Ca, and Sr were calculated in a cubic lattice with lattice constants large enough to exclude any possible interaction of atoms in the lattice.

The calculations of the work functions of the corresponding perovskite materials followed a previously published procedure [42]. Supercells with 98 atoms ($8 \times 4 \times 4$ atomic layers) with a 15-Å vacuum layer were selected and computed with the same computational parameters and distribution of bare+Hartree potentials within the unit cell in QUANTUM ESPRESSO. The high dipolar nature of the material with positively charged octahedrons and negatively charged MA cations together with different dipolar orientations of the MA cations inside the lattice makes it difficult to find a stable absolute reference for the vacuum level in the DFT calculations. (Details of calculations are reported in the Supplemental Material [43].) The calculated energy levels for different alkaline-earth-metal perovskites, however, agree well with theoretical predictions and tight-binding approximation interpretations.

The x-ray diffraction (XRD) data was simulated in the DIAMOND software using the wavelength of Cu $K\alpha$ radiation. The simulations were based on the atomic coordinates from the relaxed DFT computed structures in this work. As a composition we also simulated an XRD pattern for $MAPbI_3$, which essentially was identical to our previously published experimental diffraction of $MAPbI_3$ [15]. DFT does not take into account the concept of temperature, which has the effect of a slightly smaller unit cell and that the organic ions lose some of their collective symmetry compared to the time-averaged structure observed in experimental XRD measurements at room temperature. This breaks the room temperature symmetry with a more preferred orientation of the organic dipolar cations at zero K and leads to a splitting of some of the diffraction peaks. The experimental XRD patterns of the alkaline-earth perovskites would have their peaks at slightly larger angles compared with that predicted at zero Kelvin and the double peaks in the simulated diffractograms would be seen as single peaks.

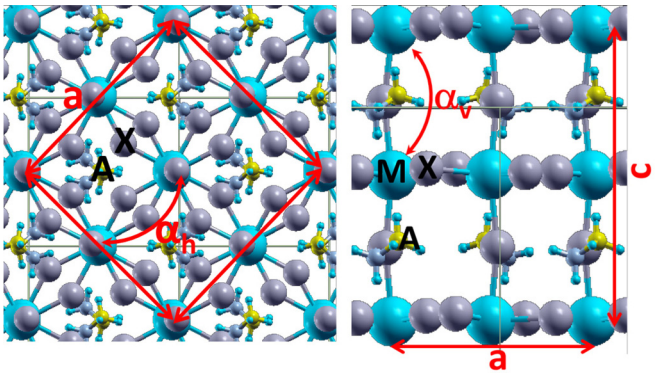

FIG. 1. Schematic of tetragonal super cell: (a) top view along the c axis and (b) side view along the b axis. Cell parameters a and c, vertical tilting angle α_v, and horizontal tilting angle α_H are depicted. The tetragonal unit cell consists of four tilted cubic unit cells as described in the Theoretical Models and Methods section. A, M, and X correspond to methylammonium, metal cation, and iodine, respectively.

III. RESULTS AND DISCUSSION

It has been proposed that the band gap of $MAPbI_3$ can be tuned by replacing the MA^+ with smaller or larger organic molecules or inorganic cations. Steric engineering of the band gap of the material by inserting different cations points at the importance of bond angles and the tilting of the lead iodide octahedrons within the perovskite lattice, which strongly affects the orbital overlap integrals and consequently, also the band gap [26].

Another important factor influencing the band gap of the perovskite materials is the electronegativity of the metal cation M, where higher electronegativity differences between the metal ion and the anion leads to a higher band gap [15,44,45]. So far, the use of different cations such as methyl ammonium, formamidinium, cesium, different metals such as strontium, tin, and bismuth, and different anions such as bromide and chloride have been investigated, either theoretically or experimentally [2,14,17,20,22,32,35,46–48]. Among the metal cations that previously have been investigated for replacing lead, we find tin, bismuth, and strontium, here extended also to include Ca and Ba.

A. Structural properties

The DFT calculations predict that stable AMX_3 perovskite phases, where A is methyl ammonium, X is iodine and M, barium, strontium, and calcium (Fig. 1), exist for all three investigated alkaline-earth metals. According to the calculations, the stable phase is tetragonal for all three alkaline-earth-metal perovskites, which conforms to the situation for the lead perovskite, $MAPbI_3$.

The formation energy differences, (ΔE_F), of the related perovskite structure are compared to $MAPbI_3$, and the corresponding relaxed cell parameters together with the bond lengths and octahedral tilting angles were calculated. These data are summarized in Table I, where more details can be found in Sec. S1 of the Supplemental Material [43].

TABLE I. Lattice parameters, tilting angle, bond length, and formation energy difference for the investigated structures.

	a(Å)	c(Å)	α_H(°)	α_v(°)	$M-X$(Å)[a]	ΔE_F kJ/mol[b]
$MAPbI_3$	8.85	12.65	153.89	170.77	6.21	0
$MACaI_3$	8.62	12.52	158.33	173.35	6.15	+157
$MASrI_3$	8.79	12.92	151.27	172.28	6.31	+163
$MABaI_3$	8.94	13.19	145.17	168.69	6.45	+212

[a]Averaged bond length considering M-M distances along the c axis and in the ab plane. See Sec. S1 of Supplemental Material [43] for all values.
[b]Calculated considering the same thermodynamic factors with crystal growth of $MAPbI_3$. Positive value means more negative formation energy for the alkaline-earth perovskites.

Considering the same thermodynamic factors for crystal formation, we noticed that the alkaline-earth perovskites are stable phases with negligible energy differences compared to the conventional lead perovskite, $MAPbI_3$ (Table I). Furthermore, the variable cell relaxation parameters of the alkaline-earth perovskites are very close to the ones of the lead perovskite, $MAPbI_3$ (Table I).

The lattice constants of the perovskite materials are changing slightly according to the atomic (ionic) radius of the metal M (presented in Table II), i.e., from calcium to barium, the corresponding perovskite lattice constants become larger. Tilting of the octahedron inside the perovskite lattice is an important parameter which is known to affect the band gap of the material [26,27]. The vertical and horizontal titling angle is here a consequence of steric effects caused by the atomic radius rather than the electronegativity of the metal ion. The tilting is highest for the calcium and lowest for the barium perovskite. That has consequences for the band gap and other physical properties of the material, as discussed in the next section.

B. Band-gap variation and band-edge shifts

Calculated density of states (DOS) for alkaline-earth-metal perovskites predicts band gaps of 2.95–3.6 eV for these materials (Table II and Fig. 2). Although DFT-calculated band gaps can be underestimated compared to experimental values, a relative comparison can be performed showing the trend in the band-gap evolution. In the hybrid perovskite

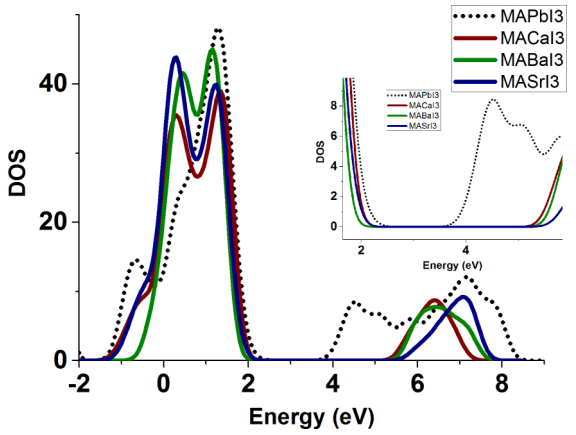

FIG. 2. Total DOS for the alkaline-earth organometallic halide perovskites ($MACaI_3$, $MABaI_3$, and $MASrI_3$). Lead iodide perovskite ($MAPbI_3$) is represented by the dashed line. Inset shows the VB and CB edges of the related perovskite materials.

materials, scalar relativistic GGA-DFT calculations have quite surprisingly been shown to give very good agreement with experimental results, as outlined in the Introduction, and are here utilized for the rare-earth halogen perovskites to calculate the band-gap variation as well as other electronic properties of the material. Apart from the most notable difference of a CB shift with lead replacement with alkaline-earth metals seen in Fig. 2, also the increase of the density of states at the CB edge is different. Here, the Sr perovskite is standing out with a less steep CB edge onset and a shift of the maximum of the density of states compared to the other alkaline-earth-metal perovskites. The VB edge of the halide perovskites are mainly composed of iodide orbitals, with little hybridization by metal orbitals, and the CB edge is mainly composed of the outermost electronic states of the metal, as can be seen in the calculated partial density of states (PDOS) in Fig. 3 and Fig. S.9 of the Supplemental Material [43]. In the PDOS, one can see that alkaline-earth-metal contribution to the CB follows the trend in work function of the metal with a minimum for Sr where the relatively large contribution from methyl ammonium is the origin of the shift of maximum of the DOS in the CB band. Here we see that it is not the electronegativity in itself which shows a monotonic decrease in the series Ca-Sr-Ba, but instead the work function of the metal that is the most important factor.

TABLE II. Atomic and ionic radius, electronegativity, work function of the corresponding elements, and calculated band gap of the related perovskites.

	Atomic radius (pm)[a]	Ionic radius^{2+} (pm)[b]	Electronegativity[c]	Work function of metal(eV)[d]	Band gap of related perovskite(eV)[e]
Pb	180	119	1.85	4.25	1.66
Ca	180	100	1.03	2.87	2.95
Sr	200	118	0.96	2.59	3.60
Ba	215	135	0.88	2.7	3.30

[a]Reference [49].
[b]Reference [50].
[c]Reference [51].
[d]Reference [52].
[e]Calculated, present work.

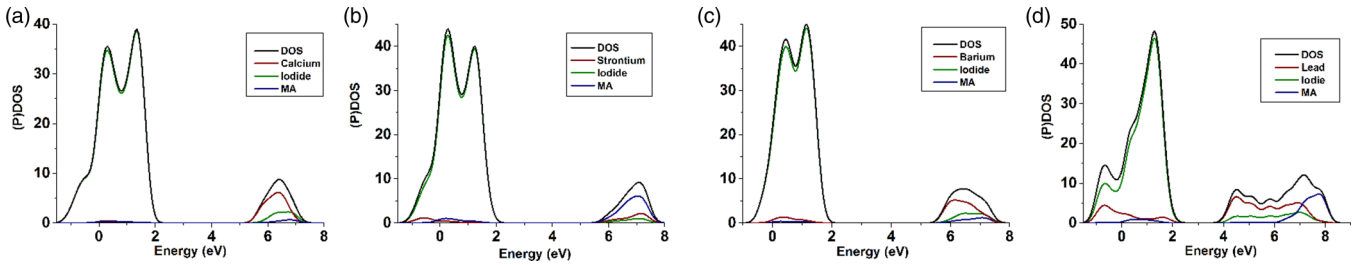

FIG. 3. PDOS of perovskite materials: (a) $MACaI_3$, (b) $MASrI_3$, (c) $MABaI_3$, and (d) $MAPbI_3$. The energy levels are not corrected versus vacuum energy level.

It has been proposed that the electronegativity of the metal M in the AMX_3 perovskite and the chemical nature of the M-X bond are important factors influencing the band gap of the material [45,47,48]. It is not the electronegativity in itself, however, that is the origin of this effect, as seen in Fig. 3 for the CB shift and contribution from metal localized orbitals. In systems with negligible hybridization of the metal orbitals, it is instead the higher work function of the metal that dictates the position of the CB edge and thereby the change of the band gap. For Ca, Sr, and Ba the work functions are 2.87, 2.56, and 2.70, respectively, which explains why the band gap decreases while going from $MACaI_3$ to $MASrI_3$ and increasing again for $MABaI_3$, whereas the electronegativity decreases monotonically for the alkaline-earth-metal series.

Although the tight-binding (TB) approximation is not an appropriate method for prediction of the full electronic structure of perovskite semiconductors, it has showed good agreement with experiments when used to explain the band shifts and band-gap variation in related perovskite materials [26]. According to the TB approximation, the periodic Hamiltonian eigenvalues [$\varepsilon(k)$] are equal to atomic electronic energy levels (E_m) with the following correction [53]:

$$\varepsilon(k) - E_m = \frac{\int \psi_m^*(r)\Delta u \psi(r) dr}{\int \psi_m^*(r)\psi(r) dr}, \qquad (1)$$

where $\Psi_m * (r)$ and $\psi(r)$ are atomic wave function and periodic wave function of electrons and Δu is the difference of the full periodic Hamiltonian with atomic potential. The integral is calculated in the unit cell. The difference between the full periodic crystal potential and the corresponding atomic potential is then the Δu averaged in the unit cell, projected to the atomic orbital cell, and normalized by the projection of periodic and atomic wave functions. In this sense, the Δu overlap integral is the governing factor for energy corrections.

Since the atomic wave functions spread only in the regions near the atom nuclei, the main part of the integral is calculated close to the atom. Based on the TB view, the Δu overlap integral is mainly responsible for the VB (mainly iodide $5p$ orbitals) shifts, and the ionization energy of the metal is responsible for the observed CB (mainly metal outermost electronic levels) shifts in Figs. 2 and 3.

Zoom-in plots of CB (metal levels) and VB (Iodide levels) edges are presented in the Supplemental Material [43]. The energetic level of the conduction band edge here thus correlates with the band gap of the perovskite. The lowest CB edge among the investigated compounds here correlates to the lowest band gap. That one belongs to the lead perovskite, as lead has higher ionization energy than the alkaline-earth metals. The rare-earth perovskites have conduction-band-edge energies that are closer together, as they have similar metal work functions (see also Table SI in the Supplemental Material [43]). It appears that even without considering the corrections of the overlap integrals given in Eq. (1) for the CB edge, the trends in a TB view are in accordance with the predictions from GGA. Plots of the averaged full potential Hamiltonian in the unit cell show the same clear trend and can be found in the Supplemental Material [43].

In perovskites with the same metal and halide atoms but where the organic ions are replaced, the tilting angle of the metal-halogen octahedron is a factor which influences the amount of orbital overlap [26] and consequently also the band gaps of the perovskite. While changing the metal ion, as is done here, it is instead the nature of metal orbitals itself that is the most important factor for the observed band-gap variation. The band edges are here not calibrated against any absolute reference level due to dipole-induced variations in the corresponding work functions (mentioned in the Methods section and the Supplemental Material [43]). However, the VB edges are very close and the CB edges show the expected trends according to the TB interpretation. The very similar lattice constants and the same considered orientation order of the methyl ammonium dipoles for these four compounds leave us with just the contribution of positive metal nuclei of the tetragonal lattice in the ionic bare potential level at infinity (mainly used for calibration of calculated levels versus vacuum [42]) as the main difference between alkaline–rare-earth-metal perovskites and results in a negligible shift in the VB.

C. Electronic structure and charge density

Plots of the charge density, the ionic bare potential, and the periodic total potential for the four investigated perovskites (bare potential, Hartree potential, exchange correlation potential) are given in Fig. 4. In the figure, the effect of the electronegativity of the metal cation in the ground-state wave function and the nature of bonds inside the crystal are clearly seen. As the electronegativity of the metal atom decreases, the nature of the bonds becomes more ionic, i.e., more charge concentrated near the atomic nuclei and less charge distributed along the bond. Consequently, the band gap increases. The same trend is seen in the bare and total potential plots as well. However, the bare potential distribution in the perovskite lattice is more extended in-between the MA and PbI_6 octahedrons [Figs. 4(a)–4(d)], while the additional potential contribution from the negative cloud of electrons

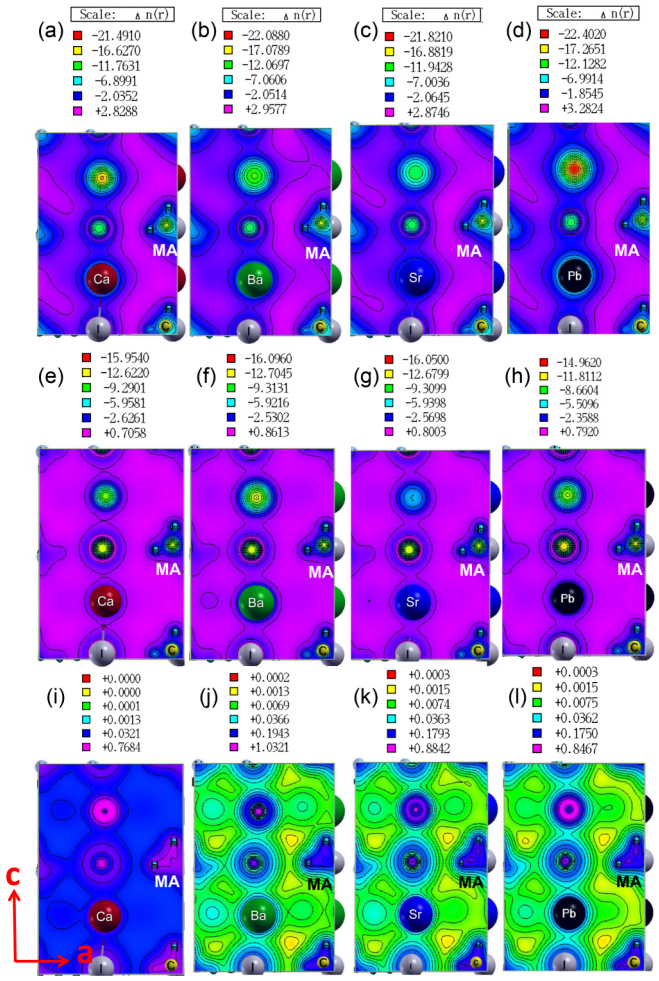

FIG. 4. Plots of bare potential (a–d), total potential (e–h), and charge density (i–l) inside the unit cell of perovskite materials $MACaI_3$ (a,e,i), $MASrI_3$ (b,f,j), $MABaI_3$ (c,g,k), and $MAPbI_3$ (d,h,l). Charge densities are plotted in the logarithmic scale from 1.0321 to 0.00 e/a_0^3 and the potentials are plotted in linear scale in the units of Rydberg.

[Figs. 4(e)–4(h)] results in a total potential distribution that is negligible in-between the MA and PbI_6 octahedrons and is more localized on MA or Pb/I, showing weak binding of MA to the PbI network.

The calculated Löwdin charges [54], which are given in Table III, are in agreement with the integrated DOS for the top of the VB in Fig. 3. The δ parameter in Table III is a measure of the difference of excess charge lying on the metal (positive charge) and iodide (negative charge) atoms in the crystal bonds. When the electronegativity difference of iodide metal increases, the δ parameter increases and the bonds have a more ionic nature, which leads to a higher band gap of the related perovskite. The expected trend for the δ parameter should follow the electronegativity of alkaline-earth metals in Table III. Calculated Löwdin charges for the $MABaI_3$ perovskite show a relative discrepancy from the expected trend. This was due to the error in the overlap between the charge density and the atomic orbitals in the QUANTUM ESPRESSO package. Integrated orbital charge-density components had 0.85 total charge density, while for other structures this number

TABLE III. Löwdin charge of metal cation and iodide anion in corresponding perovskite structure expressed as the multiples of the electron elementary charge e.

	Metal charge	Iodide charge	δ	Electronegativity of metal
Pb	81.65	53.37	0.7	1.85
Ca	19.44	53.42	0.96	1.03
Sr	36.43	53.68	1.23	0.96
Ba[a]	56.63	53.04	–	0.88

[a]The accuracy of wave-function projection to atomic orbitals was lower for the Ba calculated by the ESPRESSO package.

was 0.98, close to the ideal number of 1. The nature of the so-called σ bonds between s electrons of rare-earth metals with iodide in comparison to the so-called π bonds of lead p electrons with iodide not only determine the band gap (investigated in Sec. B) but also affects the effective mass of charge carriers, which is investigated below.

Band structure calculation of the corresponding perovskite materials, which is given in Fig. 5, show that all of them have a direct band gap in the Γ point. The calculated band gaps are unfortunately a bit high for those materials to be efficient photoabsorbers. In essence, that is a consequence of the lower electronegativity of the alkaline-earth metals that makes the VB bonds more ionic in nature, which in turn favors π bonds instead of σ bonds between the metal and the halogen. Since

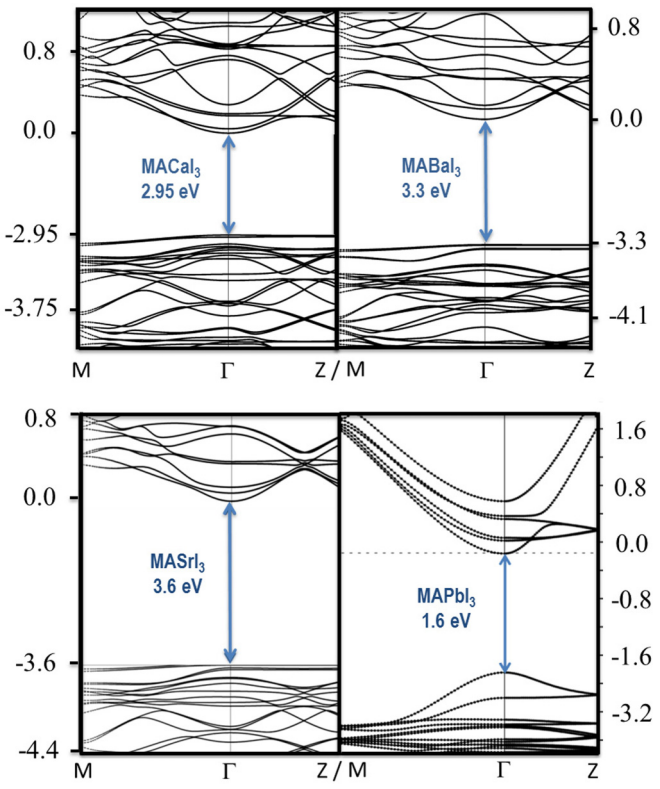

FIG. 5. Calculated band structure of the perovskite materials along the M -Γ-Z path for (a) $MACaI_3$, (b) $MABaI_3$, (c) $MASrI_3$, and (d) $MAPbI_3$. Apart from $MAPbI_3$, the energy scale labels are valid just for CB and VB and not for the band gap.

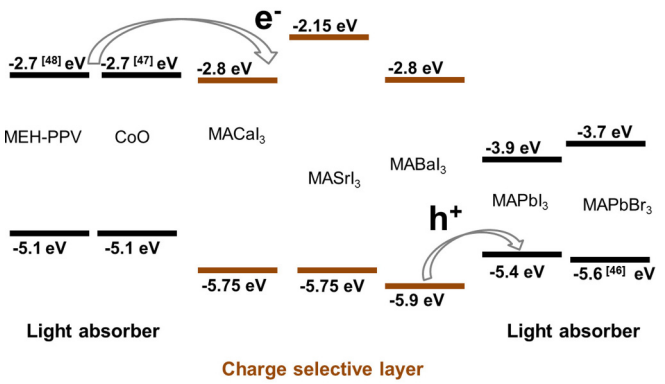

FIG. 6. Energy levels of alkaline-earth and lead metalorganic halide perovskites versus vacuum level. Light absorber candidates with proper band edges that can be implemented together with alkaline-earth perovskites for both electron and hole transporting purposes are introduced. Experimental values of $MAPbBr_3$, CoO, and MEH-PPV are adopted from Refs. [55–57], respectively, and the $MAPbI_3$ value is from Ref. [16].

the (Pauli) electronegativity is defined as a measure of electron affinity for elements within a covalent bond, it is a problematic measure for metals with delocalized states unless they are hybridized. Here, we see that it is instead the work function of the metal that dictates the details of the CB upshift and then slight downshift instead of the monotonically decreased electronegativity in the series Pb-Ca-Sr and Ba.

The curvatures of the parabola close to the valence band edge seen in Fig. 5 indicate a very high effective mass for the holes in the alkaline-earth perovskites. Fitting of the band dispersion between the Γ point and M direction in the compounds gave a very similar effective electron mass of $0.41m_0$ and an effective hole mass of $9.6m_0$ for the alkaline-earth metals. (For details of the fitting, see Supplemental Material [43].) This can be compared to the situation for the $MAPbI_3$, which gave $0.21m_0$ and $0.18m_0$ for the effective electron and hole masses, respectively.

The close-to-flat VB situation and thus the high effective mass of the holes can be detrimental for the hole-conducting properties if a too-thick layer is used. The position of the energy levels and the calculated work functions, however, do show that they can be used as p-type selective layers that may be able to accept holes from $MAPbI_3$ and energetically reject any electrons from it. The same crystalline structure and the extremely close similarity of the lattice constant of these materials compared to $MAPbI_3$ are beneficial factors of these possible hole selective layers. The effective mass of the holes, however, is predicted to be high, and the utilization requires a thin layer to be able to effectively transfer the holes. In practice, this can be of less concern, since the hole and electron selective contacts can be very thin in a working solar cell. The layer would instead lead to epitaxial growth of high-quality $MAPbI_3$ films on these materials. This would potentially also minimize the lattice mismatch and strain between the device layers and thus minimize this as a source of backcontact recombination. If the holes instead are transported with hole hopping via shallow defects, the high effective mass of the hole is less of a problem.

Considering thicker films, differences between electron and hole effective masses instead make them interesting candidates for electron selective contacts if the energy-level alignment with photoabsorber is matched, a situation that is desirable in hot carrier injection devices that require rather high CB acceptor levels. Oxide light absorbers and some organic absorbers have high CB edges that result in large potential losses when they employ conventional electron transporting materials. Alkaline-earth perovskites in the latter case are capable of playing key roles as transparent, highly electron conductive layers with proper and tunable band edges.

In Fig. 6, the calculated band edges for alkaline-earth-metal perovskites, the $MAPbI_3$ reference compound, as well as a few light absorber candidates for both electron and hole-conducting purposes are presented. The levels are calibrated against the vacuum layer according to the experimental value of the $MAPbI_3$ band edges, considering a similar ionic bare potential for these compounds with $MAPbI_3$, as discussed in Sec. III B. Although the absolute CB edge should be taken with care until experimental efforts show the measured values, it gives important insight regarding the relative trends and mechanism of how the different cations change the electronic structure. The absolute values in experiments can also be further fine-tuned through halogen or organic cation exchange and could be less of a problem with slightly mismatched CB values from a practical point of view.

D. Remarks about the synthesis of the perovskites

Initial experimental attempts to synthesize the methyl ammonium barium iodide ($MABaI_3$), methyl ammonium strontium iodide ($MASrI_3$), and methyl ammonium calcium iodide ($MACaI_3$) were performed.

Lower solubility and different crystal structure of the metal-halogen precursor compared to PbI_2 resulted in fast growth of a nonlayered structure precursor that impeded the intercalation of highly soluble MA^+ ions inside, which consequently obstructed formation of the perovskites (Sec. S3 of Supplemental Material [43]).

However, as suggested previously, vapor phase growth should be a plausible technique for the synthesis of these types of compounds [15] that are theoretically predicted to have similar formation energies with $MAPbI_3$. Theoretically predicted XRD spectra for these compounds are presented in Fig. 7. Those are based on the DFT optimized lattice constant and atomic coordinates and can be used to verify experimental diffraction of these new compounds. A different cation size of the metals leads to different lattice constants of the corresponding perovskite (presented in Table I), which is reflected in the position of related XRD peaks (Fig. S6.c of Supplemental Material [43]).

The synthesis of a system with a mixed perovskite with both lead and alkaline-earth metals was also pursued but also not fully accomplished, and suffered from the same difficulties as for the pure alkaline-earth perovskite synthesis mentioned above (Sec. S4 of Supplemental Material [43]). The same cationic charge and size of the suggested alkaline-earth metals compared to lead together with theoretically predicted similar formation energy of the corresponding perovskites opens up the possibility of partial replacement of lead with

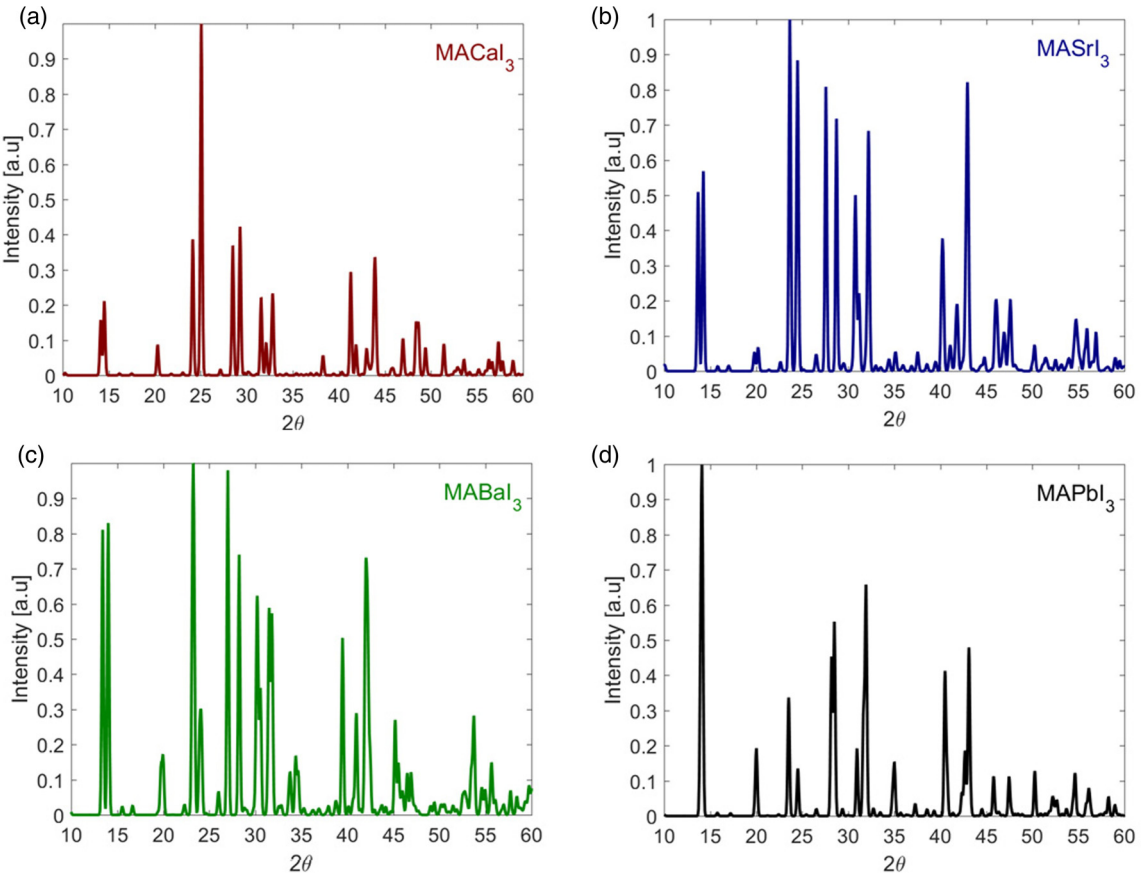

FIG. 7. Predicted XRD peaks for (a) $MACaI_3$, (b) $MASrI_3$, (c) $MABaI_3$, and (d) $MAPbI_3$.

alkaline-earth metal in the perovskite lattice. This can be beneficial from different aspects such as tuning the band gap, making colorful devices and having less toxic content.

IV. CONCLUDING REMARKS

In summary, a series of alkaline-earth metalorganic perovskite materials was investigated for solar cell applications. Electronic band structures and PDOS spectra are studied, along with the presence of both hole selective materials with the same lattice constant and crystal structure of $MAPbI_3$ and electron selective material for high-band-edge light absorbers in solar cell applications. A p-type contact with the same lattice constants as the perovskite used as a photoabsorber would potentially be highly beneficial for high-quality crystalline growth of $MAPbI_3$ in an inverted device configuration. It could also potentially reduce the interface mismatches and thus minimize these sources of backcontact recombination. Our theoretical results indicate that the alkaline-earth perovskites could be such materials, given that they can be synthesized and applied as a thin layer and not have any other detrimental properties not here considered.

Periodic DFT calculations together with single atomic calculations and tight-binding approximation were implemented to illuminate the mechanism of the band-edge shifts and band-gap variation in the investigated materials with metal cation exchange. The electronegativity and work-function difference of the metal and iodide play a key role in the band-gap tuning rather than the tilting angles of the metal-halogen octahedral. Higher electronegativity of the metal generally results in lower band gaps where the work function of the metal is found to be the single most important factor. The effective masses of the electrons were found to be reasonably low ($0.41m_0$), whereas the effective masses for the holes were very large ($9.6m_0$). (See Sec. S.7 of Supplemental Material [43] for the details.) This indicates that thin layers of these materials are required if they are to be used as hole selective materials. Overlap integrals of the periodic Hamiltonian between the molecular orbitals of iodide and the metal cations are responsible for the CB and VB band shifts observed in the DOS spectrum. The Löwdin charges of the atoms in the lattice were in agreement with the concept that at higher electronegativity differences between the metal and the halogen leads to more ionic bonds and higher band gaps. As a summary of our calculations, the estimated energy levels of alkaline-earth perovskites in comparison to $CH_3NH_3PbI_3$, together with some light absorber candidates for both electron and hole selective layer applications are illustrated in Fig. 6.

ACKNOWLEDGMENTS

We acknowledge Uppsala Multidisciplinary Center for Advanced Computational Science (UPPMAX) for providing the computational resources under Project snic 2015-6-65 and

snic 2015-1-281. The Swedish Energy Agency and STandUP for Energy Program are acknowledged for foundation support. M.P. acknowledges Jolla Kullgren and Matthew Wolf for their helpful discussions about the work-function calculations.

[1] M. D. McGehee, Nat. Mater. **13**, 845 (2014).
[2] N. J. Jeon, J. H. Noh, W. S. Yang, Y. C. Kim, S. Ryu, J. Seo, and S. Il Seok, Nature (London) **517**, 476 (2015).
[3] W. S. Yang, J. H. Noh, N. J. Jeon, Y. C. Kim, S. Ryu, J. Seo, and S. Il Seok, Science **348**, 1234 (2015).
[4] M. M. Lee, J. Teuscher, T. Miyasaka, T. N. Murakami, and H. J. Snaith, Science **338**, 643 (2012).
[5] H.-S. Kim, C.-R. Lee, J.-H. Im, K.-B. Lee, T. Moehl, A. Marchioro, S.-J. Moon, R. Humphry-Baker, J.-H. Yum, J. E. Moser, M. Grätzel, and N.-G. Park, Sci. Rep. **2**, 591 (2012).
[6] S. D. Stranks, P. K. Nayak, W. Zhang, T. Stergiopoulos, and H. J. Snaith, Angew. Chemie Int. Ed. **54**, 3240 (2015).
[7] F. T. F. O'Mahony, Y. H. Lee, C. Jellett, S. Dmitrov, D. T. J. Bryant, J. R. Durrant, B. C. O'Regan, M. Graetzel, M. K. Nazeeruddin, and S. A. Haque, J. Mater. Chem. A **3**, 7219 (2015).
[8] F. K. Aldibaja, L. Badia, E. Mas-Marzá, R. S. Sánchez, E. M. Barea, and I. Mora-Sero, J. Mater. Chem. A **3**, 9194 (2015).
[9] M. Grätzel, Nat. Mater. **13**, 838 (2014).
[10] J. Schoonman, Chem. Phys. Lett. **619**, 193 (2015).
[11] K. G. Stamplecoskie, J. S. Manser, and P. V. Kamat, Energy Environ. Sci. **8**, 208 (2015).
[12] J. S. Manser and P. V Kamat, Nat. Photonics **8**, 737 (2014).
[13] A. Marchioro, J. Teuscher, D. Friedrich, M. Kunst, R. van de Krol, T. Moehl, M. Grätzel, and J.-E. Moser, Nat. Photonics **8**, 250 (2014).
[14] F. Hao, C. C. Stoumpos, D. H. Cao, R. P. H. Chang, and M. G. Kanatzidis, Nat. Photonics **8**, 489 (2014).
[15] T. J. Jacobsson, M. Pazoki, A. Hagfeldt, and T. Edvinsson, J. Phys. Chem. C **119**, 25673 (2015).
[16] P. Gao, M. Grätzel, and M. K. Nazeeruddin, Energy Environ. Sci. **7**, 2448 (2014).
[17] G. E. Eperon, S. D. Stranks, C. Menelaou, M. B. Johnston, L. M. Herz, and H. J. Snaith, Energy Environ. Sci. **7**, 982 (2014).
[18] S. Lv, S. Pang, Y. Zhou, N. P. Padture, H. Hu, L. Wang, X. Zhou, H. Zhu, L. Zhang, C. Huang, and G. Cui, Phys. Chem. Chem. Phys. **16**, 19206 (2014).
[19] N. Pellet, P. Gao, G. Gregori, T.-Y. Yang, M. K. Nazeeruddin, J. Maier, and M. Grätzel, Angew. Chem. Int. Ed. Engl. **53**, 3151 (2014).
[20] M. Safdari, A. Fischer, B. Xu, L. Kloo, and J. M. Gardner, J. Mater. Chem. A **3**, 9201 (2015).
[21] N. K. Noel, S. D. Stranks, A. Abate, C. Wehrenfennig, S. Guarnera, A.-A. Haghighirad, A. Sadhanala, G. E. Eperon, S. K. Pathak, M. B. Johnston, A. Petrozza, L. M. Herz, and H. J. Snaith, Energy Environ. Sci. **7**, 3061 (2014).
[22] E. Edri, S. Kirmayer, D. Cahen, and G. Hodes, J. Phys. Chem. Lett. **4**, 897 (2013).
[23] F. C. Hanusch, E. Wiesenmayer, E. Mankel, A. Binek, P. Angloher, C. Fraunhofer, N. Giesbrecht, J. M. Feckl, W. Jaegermann, D. Johrendt, T. Bein, and P. Docampo, J. Phys. Chem. Lett. **5**, 2791 (2014).
[24] C. C. Stoumpos, C. D. Malliakas, and M. G. Kanatzidis, Inorg. Chem. **52**, 9019 (2013).
[25] A. Stroppa, D. Di Sante, P. Barone, M. Bokdam, G. Kresse, C. Franchini, M.-H. Whangbo, and S. Picozzi, Nat. Commun. **5**, 5900 (2014).
[26] M. R. Filip and F. Giustino, Nat. Commun. **5**, 1 (2014).
[27] A. Amat, E. Mosconi, E. Ronca, C. Quarti, P. Umari, M. K. Nazeeruddin, M. Grätzel, and F. De Angelis, Nano Lett. **14**, 3608 (2014).
[28] C. Quarti, E. Mosconi, and F. De Angelis, Chem. Mater. **26**, 6557 (2014).
[29] V. M. Goldschmidt, Naturwissenschaften **14**, 477 (1926).
[30] G. Kieslich, S. Sun, and T. Cheetham, Chem. Sci. **6**, 3430 (2015).
[31] I. Borriello, G. Cantele, and D. Ninno, Phys. Rev. B **77**, 235214 (2008).
[32] E. Mosconi, A. Amat, K. Nazeeruddin, M. Gra, and F. De Angelis, J. Phys. Chem. C **117**, 13902 (2013).
[33] L. Abbes and H. Noura, Results Phys. **5**, 38 (2015).
[34] J. Even, L. Pedesseau, M. A. Dupertuis, J. M. Jancu, and C. Katan, Phys. Rev. B: Condens. Matter Mater. Phys. **86**, 3 (2012).
[35] P. Umari, E. Mosconi, and F. De Angelis, Sci. Rep. **4**, 4467 (2014).
[36] J. Even, L. Pedesseau, and C. Katan, Proc. SPIE **9140**, 91400Y (2014).
[37] M. R. Filip and F. Giustino, Phys. Rev. B **90**, 245145 (2014).
[38] P. Giannozzi, S. Baroni, N. Bonini, M. Calandra, R. Car, C. Cavazzoni, D. Ceresoli, G. L. Chiarotti, M. Cococcioni, I. Dabo, A. Dal Corso, S. de Gironcoli, S. Fabris, G. Fratesi, R. Gebauer, U. Gerstmann, C. Gougoussis, A. Kokalj, M. Lazzeri, L. Martin-Samos *et al.*, J. Phys.: Condens. Matter **21**, 395502 (2009).
[39] J. P. Perdew, K. Burke, and M. Ernzerhof, Phys. Rev. Lett. **77**, 3865 (1996).
[40] J. P. Perdew, K. Burke, and Y. Wang, Phys. Rev. B **54**, 16533 (1996).
[41] A. Kokalj, Comput. Mater. Sci. **28**, 155 (2003).
[42] M. Pazoki, N. Nafari, and N. Taghavinia, RSC Adv. **4**, 301 (2014).
[43] See Supplemental Material at http://link.aps.org/supplemental/10.1103/PhysRevB.93.144105 for relaxation parameters of perovskite lattices, numerically averaged total potential and charge density of corresponding perovskite lattices, efforts for the experimental synthesis of pure alkaline-earth perovskite and mixed alkaline-earth and lead perovskites, zoom-in plots of PDOS, and details of the work-function and effective mass calculations.
[44] F. Wang, I. Grinberg, and A. M. Rappe, Appl. Phys. Lett. **104**, 152903 (2014).
[45] D. Mekam, S. Kacimi, M. Djermouni, M. Azzouz, and A. Zaoui, Results Phys. **2**, 156 (2012).
[46] C. Katan, L. Pedesseau, M. Kepenekian, A. Rolland, and J. Even, J. Mater. Chem. A **3**, 9232 (2015).
[47] C. Grote, B. Ehrlich, and R. F. Berger, Phys. Rev. B **90**, 205202 (2014).
[48] I. E. Castelli, J. M. García-Lastra, K. S. Thygesen, and K. W. Jacobsen, APL Mater. **2**, 081514 (2014).

[49] J. C. Slater, J. Chem. Phys. **41**, 3199 (1964).
[50] R. D. Shannon, Acta Cryst. **A32**, 751 (1976).
[51] L. C. Allen, J. Am. Chem. Soc. **111**, 9003 (1989).
[52] H. B. Michaelson, J. Appl. Phys. **48**, 4729 (1977).
[53] D. N. Ashcroft and N. W. Mermin, *Solid State Physics* (Brooke Cole, NY, 1976).
[54] A. Fallis, J. Chem. Inf. Model. **53**, 1689 (2013).
[55] B. Park, B. Philippe, S. M. Jain, X. Zhang, T. Edvinsson, H. Rensmo, B. Zietz, and G. Boschloo, J. Mater. Chem. A **3**, 21760 (2015).
[56] Y. F. Zhou, M. Eck, and M. Kruger, Energy Environ. Sci. **3**, 1851 (2010).
[57] M. T. Greiner, M. G. Helander, W. M. Tang, Z. B. Wang, J. Qiu, and Z.H. Lu, Nat. Mater. **11**, 76 (2011).